Expansion microscopy: principles and uses in biological research

Asmamaw T. Wassie[1,2,3,4,8], Yongxin Zhao[4,5,8] and Edward S. Boyden[1,2,3,4,6,7]*

Many biological investigations require 3D imaging of cells or tissues with nanoscale spatial resolution. We recently discovered that preserved biological specimens can be physically expanded in an isotropic fashion through a chemical process. Expansion microscopy (ExM) allows nanoscale imaging of biological specimens with conventional microscopes, decrowds biomolecules in support of signal amplification and multiplexed readout chemistries, and makes specimens transparent. We review the principles of how ExM works, advances in the technology made by our group and others, and its applications throughout biology and medicine.

Optical microscopy techniques make up one of the most important toolsets in the history of biology and medicine. Until recently the diffraction limit posed by physics limited the resolution of optical microscopes to values of a few hundred nanometers—far greater than the size of biological molecules. The development of near-field imaging[1,2] and a suite of far-field super-resolution microscopy techniques[3,4] have enabled researchers to optically image single molecules and nanoscale structures in biology. Although powerful, such technologies typically require expensive equipment and/or have slow imaging speeds; 3D super-resolution imaging, especially of specimens of tissues and organs, remains a challenge. Recently we discovered that it is possible to physically magnify a preserved biological specimen[5] in an even fashion by synthesizing a dense, cross-linked network of swellable polyelectrolyte hydrogel throughout such a specimen (Fig. 1a). This in turn can smoothly and isotropically expand biomolecules or labels away from each other after chemical processing. After such physical magnification, molecules in a diffraction-limited region are separated in space to greater distances, and therefore can be resolved even by conventional diffraction-limited microscopes.

The ExM approach brings together two different fields: the physics of swellable polyelectrolyte hydrogels, which vastly increase in size when immersed in a solvent such as water and which were explored in depth by groups such as that of Toyoichi Tanaka in the late 1970s[6], and the embedding of preserved biological specimens in polymer hydrogels for imaging purposes, pioneered by teams such as that of Peter Hausen and Christine Dreyer, who used uncharged polyacrylamide hydrogels to facilitate tissue staining and imaging in the early 1980s[7]. Such gels have polymer spacings (or mesh sizes) that are quite small—approximately 1–2 nm (ref. [8])—which leads us to think that the errors introduced by in situ polymerization and expansion could in principle also be quite small, perhaps on the order of the size of a biomolecule.

Over the past few years, we have developed a diversity of ExM protocols that enable imaging of proteins[9] and RNAs[10], that can physically magnify objects multiple times in succession to achieve very high resolution[11], or that can be applied to human clinical specimens[12]. Other groups have independently developed analogous chemistries for the visualization of proteins[13–15] and RNAs[16] in expanded samples. We here review the progress in this rapidly developing and increasingly widely adopted technique. We discuss the principles of ExM, how ExM is being applied in biology and medicine, and future directions for the technology and its application.

All ExM protocol variants share a similar logical flow, essential for isotropic specimen expansion, that preserves biological information down to nanoscopic length scales (Fig. 1b). The design of the chemistry is aimed at ensuring the greatest degree of isotropy possible during the expansion process. First, molecular handles are covalently attached to biomolecules and/or labels (Fig. 1b, step i) that enable them to be bound to a swellable hydrogel synthesized throughout the specimen. Second, the specimen is immersed in a monomer solution (containing sodium acrylate) that reacts via free-radical polymerization to form a densely cross-linked (via the cross-linker N-N'-methylenebisacrylamide) and highly penetrating polyelectrolyte hydrogel (sodium polyacrylate). This surrounds the biomolecules and/or labels, binding to the molecular handles so that the attached biomolecules and/or labels are mechanically coupled to the polymer mesh (Fig. 1b, step ii). Third, the specimen is homogenized with respect to its mechanical properties by chemical denaturation via heat and detergent treatment, or by enzymatic digestion, as appropriate for the specimen and the molecules to be visualized (Fig. 1b, step iii). Finally, the specimen is immersed in water, which diffuses into the polyelectrolyte hydrogel through osmotic force, causing swelling that is facilitated by the highly charged nature of the polyelectrolyte mesh. (Fig. 1b, step iv). After expansion, further labels and/or amplification chemistries to improve visualization may be applied.

Most ExM protocols expand a biological specimen by about 100× in volume, or ~4.5× in the linear dimension; this factor is set by the cross-linker concentration (reduction of the cross-linker concentration results in greater gel expansion factors, but also greater gel fragility; recently a protocol using the additional monomer N,N-dimethylacrylamide acid during the polymerization step

[1]Department of Brain and Cognitive Sciences, Massachusetts Institute of Technology, Cambridge, MA, USA. [2]Department of Biological Engineering, Massachusetts Institute of Technology, Cambridge, MA, USA. [3]McGovern Institute, Massachusetts Institute of Technology, Cambridge, MA, USA. [4]Media Lab, Massachusetts Institute of Technology, Cambridge, MA, USA. [5]Department of Biological Sciences, Carnegie Mellon University, Pittsburgh, PA, USA. [6]Koch Institute, Massachusetts Institute of Technology, Cambridge, MA, USA. [7]Center for Neurobiological Engineering, Massachusetts Institute of Technology, Cambridge, MA, USA. [8]These authors contributed equally: Asmamaw T. Wassie and Yongxin Zhao. *e-mail: esb@media.mit.edu
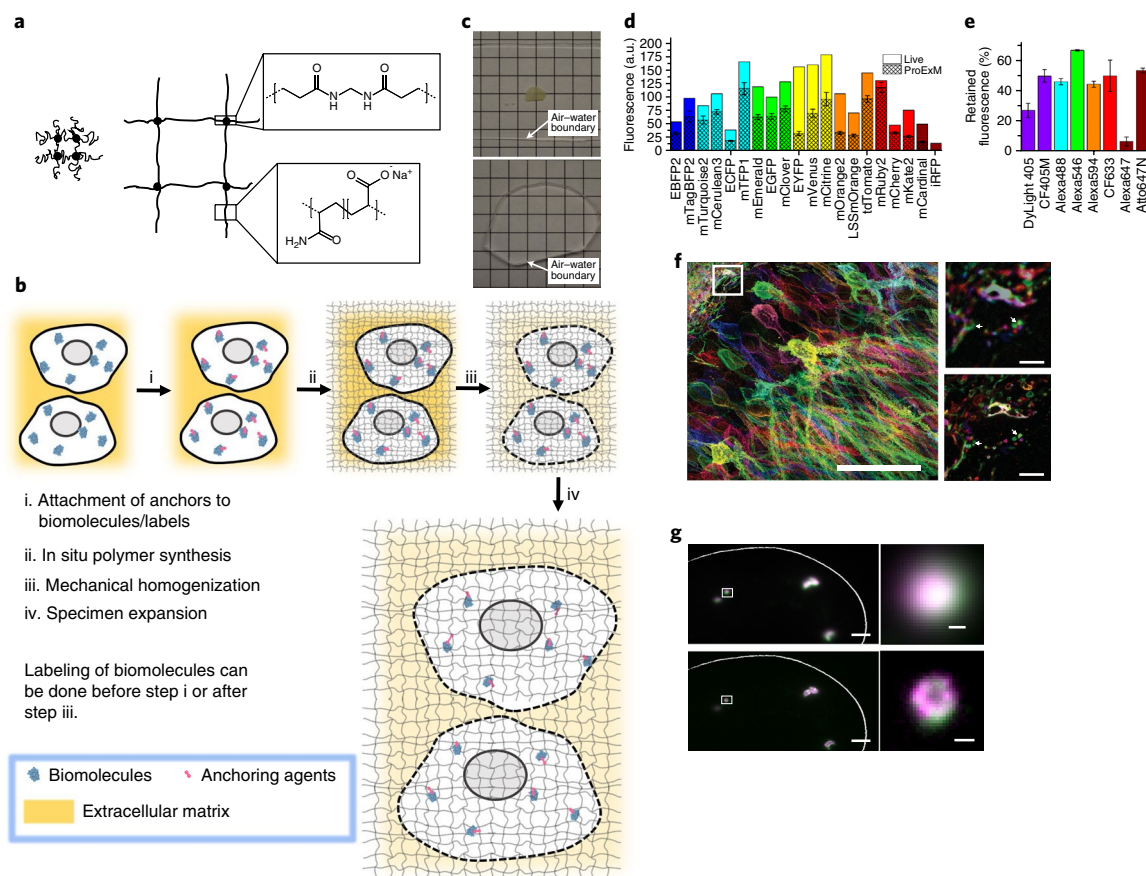
Fig. 1 | ExM concept and example outcomes. a, Schematic of the ExM polyelectrolyte hydrogel, cross-linked sodium polyacrylate, showing the cross-linker (dots) and polymer chain (lines) in the collapsed state before expansion (left) and in the expanded state (right). Chemical structures of cross-linker and monomer components, in the synthesized polymer context, are shown on the right. **b**, Diagram showing the generalized workflow for ExM. Not to scale. **c**, A 200-µm-thick fixed mouse brain slice before expansion (top) and after (bottom). Panels **a** and **c** adapted with permission from ref. [5], AAAS. **d**, Literature values of brightness for fluorescent proteins normalized to EGFP (open bars), compared with literature values of brightness multiplied by the observed retention percentage of each fluorescent protein with proExM (cross-hatched bars). a.u., arbitrary fluorescence units. Data are shown as the mean ± s.d. of $n = 4$ samples. **e**, Retention of fluorescent-dye-conjugated antibodies after proExM (mean ± s.d.; $n = 3$ samples). **f**, Left, mouse hippocampus expressing virally delivered Brainbow3.0 epitopes, stained with fluorescent antibodies, and then expanded via proExM; the image shows a maximum-intensity projection of a high-resolution confocal microscopy stack. Top right, pre-expansion image of the boxed region in the image on the left. Arrows indicate features highlighted in the image on the bottom right, which is a post-expansion image of the sample shown in the top right image. Panels **d**–**f** adapted with permission from ref. [9], Springer Nature. **g**, Left, smFISH images of a HeLa sample before expansion (top left) and after expansion and processing with the ExFISH protocol (bottom left), highlighting NEAT1 long noncoding RNA in the nucleus of a HeLa cell. Magenta and green indicate probe sets binding to different parts of NEAT1. Right, a NEAT1 cluster (corresponding to the boxed regions in the images on the left) imaged with smFISH (upper right) and ExFISH (bottom right). Adapted with permission from ref. [10], Springer Nature. Scale bars, 50 µm (**f**, left (physical size post-expansion, 198 µm)), 5 µm (**f**, right (physical size post-expansion for bottom right, 19.8 µm)), 2 µm (**g**, left (physical size post-expansion for bottom left, 6.6 µm)), or 200 nm (**g**, right (physical size post-expansion for bottom right, 660 nm)).

presented an ~10× linear expansion)[5,15]. With 4.5× linear expansion, a microscope with a diffraction limit of ~300 nm would attain an effective resolution of ~300 nm/4.5 ≈ 70 nm. It is also possible to expand specimens twice in series, thus enabling an ~4.5 × 4.5 ≈ 20× increase in linear dimension, so that a conventional diffraction-limited microscope could achieve a resolution of 300/20 ≈ 15 nm (in practice, this value is slightly larger owing to the size of the fluorescent labels applied to the specimen before expansion)[11], which is comparable to that of the best previous super-resolution methods for imaging of cells and tissues. Protocols are available on the web (http://expansionmicroscopy.org) and in step-by-step peer-reviewed form[17].

ExM protocols have been empirically validated by comparison of the resulting images to those obtained via previous super-resolution technologies (for example, structured illumination microscopy, stochastic optical reconstruction microscopy, and stimulated

emission depletion microscopy) followed by analysis of the distortion that results from the expansion process via a nonrigid registration algorithm, as well as by examination of post-expansion images of highly stereotyped structures (e.g., microtubules)[5,9,11–13,15,18]. The protocols we describe all exhibit low distortions of a few percent over length scales of tens to hundreds of micrometers. From an end-user perspective, the sample-to-sample reliability for a well-tested protocol is consistent enough that new biological studies are able to use well-tested protocols without further validation, especially for a cell or tissue type that has been previously validated. For a cell or tissue type being explored for the first time, validation of isotropy via the aforementioned methods may be helpful. Because user error of course can occur, it is helpful to have a quick check to evaluate protocol success; in our experience, if the overall expansion factor for a new sample matches that described in the literature for that protocol and sample type, and if no cracks or apparent deformations

occur, then there is a high likelihood that the process went well. In principle, the expansion process evenly pulls apart anchored biomolecules and/or labels while preserving the spatial organization of biomolecules relative to one another, down to a precision that we have estimated to be as small as 5–10 nm (ref. [11]) (note that this is an estimate of the error in the location of gel-anchored biomolecules introduced by polymerization and expansion that has not actually been achieved as a practical resolution to date, owing to the larger size of the labels (i.e., antibodies) used).

Because the ExM sample-preparation method enables nanoscale imaging with commonly available microscopes, it can be readily deployed in many contexts in biology and medicine. ExM also has other advantages. For example, because the final product is ~99% water, with endogenous material diluted 100× or more, it is transparent (Fig. 1c), with nearly 100% light transmission through a 200-μm-thick slice of expanded brain tissue[5]. This allows for the use of very fast imaging modalities such as light-sheet microscopy for large-volume nanoscopy[10,19]. In addition, the expansion process is compatible with the visualization of a variety of biomolecules (for example, proteins (Fig. 1d,e) and RNA (Fig. 1g)) with existing labels or stains, which means that it can push many existing techniques, such as the popular 'Brainbow' method of barcoding neurons in vivo with different fluorescent proteins or epitopes[9] (Fig. 1f), into the super-resolution realm.

Ever since our original demonstration of isotropic cell and tissue expansion in 2015, variants have been developed by our group and by other groups to enable the imaging of proteins labeled with conventional antibodies or fused to genetically encoded fluorophores (protein-retention ExM (proExM) protocols[9,13–15]), to support the imaging of RNAs labeled with fluorescence in situ hybridization (FISH) probes (expansion FISH (ExFISH)[10,16]), to enable extremely fine-resolution imaging through repeated expansion of a sample (iterative ExM (iExM)[11]), and to study human specimens such as those generated for pathology and diagnosis purposes (expansion pathology (ExPath)[12]).

Interestingly, tissue expansion was sometimes commented on in early studies of brain clearing. For example, in 2011, the Sca*l*e brain-clearing protocol (involving chemicals such as urea and Triton X-100) was noted to cause 1.25× expansion of tissues[20]. Later brain-clearing protocols such as CUBIC[21] (also involving a cocktail of small-molecule chemicals) and CLARITY[22] (also involving uncharged polyacrylamide hydrogels) also commented on swelling of tissues thus treated. In these studies, however, expansion was treated as an uncontrolled and/or undesired process, and no attempts were made to design the strategy for isotropic expansion, or to analyze whether the strategy preserved nanoscale information. However, recently, an extension of CUBIC called CUBIC-X, which applies the small molecules imidazole and antipyrine to achieve swelling of CUBIC-processed tissue, was shown to swell brain tissue ~2× linearly, thus enabling subcellular-resolution imaging of entire mouse brains with light-sheet microscopy[23].

ExM methods

Protein-retention expansion microscopy. The first version of ExM[5] (which we now call ExM 1.0) required end users to synthesize their own labeling reagents for tagging proteins of interest, which limited its utility for everyday biology contexts (although it was used for the visualization of biomolecules in *Escherichia coli*[24] (Fig. 2a)). In proExM[9], in contrast, only off-the-shelf chemicals are needed to directly retain endogenous proteins and/or exogenous protein-based labels. Two other groups—the Vaughan lab and the Chung lab—independently developed related chemistries[13,14], which we describe in more detail below. In proExM, application of the succinimidyl ester of 6-((acryloyl)amino)hexanoic acid (acryloyl-X, SE; abbreviated as AcX) to a preserved specimen equips amines on proteins with a polymerizable carbon–carbon double bond[9], which in turn enables

proteins to be anchored to the polymer during the polymerization step (Fig. 1b). The procedures below can take, depending on the protocol used and the size of the tissue to be processed, anywhere from a day to a week, with much of the time required being incubation time that permits chemical access to the tissue. Fluorescent labels for the visualization of proteins—for example, fluorescently tagged antibodies—can be applied either before or after expansion.

In the former case, standard fluorescent antibodies are applied to fixed cells or tissues before expansion occurs. Genetically encoded fluorophores, perhaps fused to proteins of interest, can also be expressed in living cells via viral delivery, transfection, or transgenesis. AcX binds to all the proteins, including the fluorescent antibodies and/or genetically encoded fluorophores. After polymerization, mechanical homogenization (Fig. 1b) is carried out by proteinase K, a powerful protease, applied at a dose that results in the destruction of the majority of the proteins that provide structural integrity to cells and tissues but spares the functions of the antibodies and fluorescent proteins[25,26]. This is possible because many antibodies and fluorescent proteins are relatively protease resistant. After gelation, digestion, and expansion, the fluorescence of the antibody labels or fluorescent proteins is largely retained for many genetically encoded fluorophore and small-molecule dyes (Fig. 1d,e), which allows for imaging of biomolecular identity and location (although the volumetric dilution due to expansion reduces the intensity per unit volume).

Most fluorescent dyes commonly used with antibodies are compatible with this process, with the exception of cyanine dyes, which are destroyed during polymerization (Fig. 1e); excellent alternatives to cyanine dyes are now available in spectral bands where cyanine dyes have been popular in the past[9]. Most GFP-like (i.e., β-barrel-structured) fluorescent proteins are also preserved in this process (Fig. 1d); infrared fluorescent proteins based on bacteriophytochromes, in contrast, are largely destroyed[9]. In addition to antibodies, other protease-resistant labels such as streptavidin can be applied pre-expansion[9]; this approach has been used to enable visualization of post-translational modifications such as S-nitrosylation that can be marked by biotin-bearing small-molecule tags[9].

In parallel to our development of proExM, another group independently developed a related protocol[13] that uses methacrylic acid N-hydroxysuccinimidyl ester (MA-NHS, which is structurally similar to AcX) or glutaraldehyde to serve as an anchor that links fluorescent proteins and antibodies to the polymer. In this study, MA-NHS was demonstrated to work well in both cultured cells and tissue slices, and glutaraldehyde was used on cultured cells. In practice, the MA-NHS protocol is fairly similar to the AcX protocol described above, as the linkers are largely analogous to one another. Further tests of the glutaraldehyde protocol on intact tissues could be conducted in the future but have not been carried out yet, to our knowledge. In this study[13], it was also shown that biotin-labeled antibodies could be used, with visualization enabled post-expansion by the application of fluorescent streptavidin, which allows for utilization of fluorophores that would have been destroyed by the expansion process, and elimination of polymerization-induced fluorophore destruction.

ProExM protocols using either AcX or MA-NHS have been validated on a wide range of fluorescent proteins and antibody-borne fluorophores, and applied to a diversity of proteins and structures (such as clathrin-coated pits, keratin fibers, actin filaments, vimentin, myelin, glial markers, chromosomes, kinetochores, mitochondria, peroxisomes, pre- and post-synaptic proteins, nuclear lamina, histones, and microtubules[9,13,18]) in a variety of cell and tissue types (including many kinds of cultured cells, as well as mouse brain, pancreas, spleen, and lung; rhesus macaque brain; and larval zebrafish[9,13,18] (Fig. 2b)). This family of protocols has very rapidly come to be used for nanoscale imaging of protein identity and location in a diversity of contexts, including for examinations of larval zebrafish
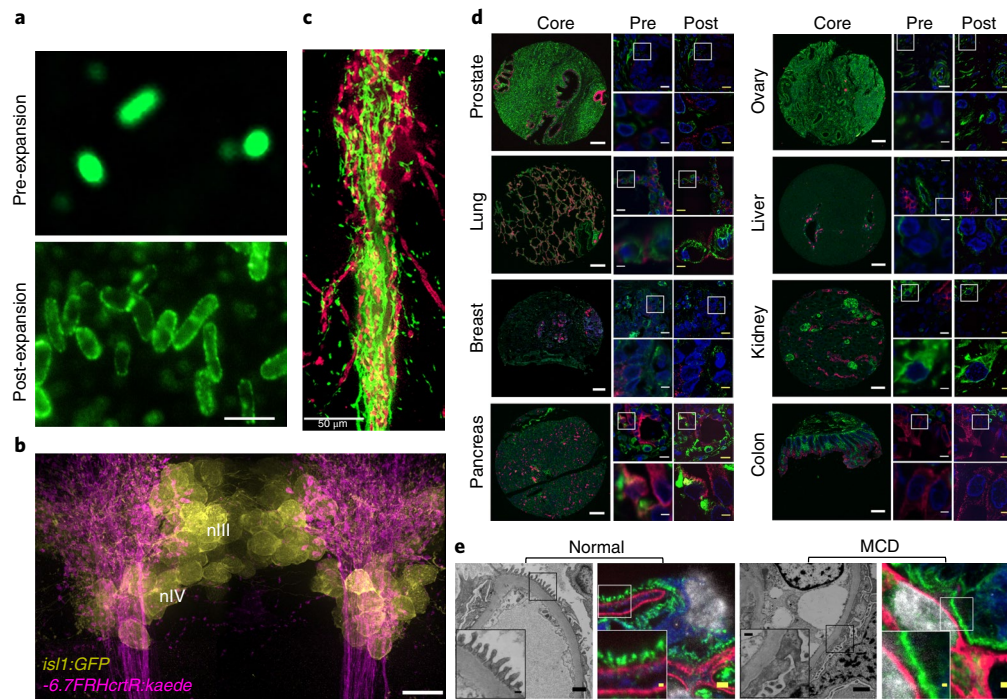
Fig. 2 | Applications of ExM in biology and medicine. a, Top, wide-field pre-expansion image of *Escherichia coli* immunolabeled for membrane lipopolysaccharides (top). Bottom, wide-field post-expansion image of *E. coli* prepared as in the top image with additional application of ExM 1.0. Reproduced with permission from ref. [24], Springer Nature. **b**, Image of part of the brain of a 6-d-old larval zebrafish (nIII and nIV refer to the nuclei of the zebrafish brain indicated; *isl1:GFP* and *-6.7FRHcrtR:kaede* refer to the fish lines used) using proExM. Image shows a maximum-intensity projection of an ~33-μm-thick volume of the brain immunolabeled for cells expressing GFP (yellow) and Kaede (magenta). Reproduced with permission from ref. [18], National Academy of Sciences. **c**, proExM image of mouse brain striatal circuits showing the intertwined 'bouquet' between striosomal fibers (green, mCitrine) and dopaminergic dendrites (magenta, tdTomato) in the mouse brain. Reproduced with permission from ref. [28], National Academy of Sciences. **d**, ExPath images of a wide range of human tissue types. A block of five images is shown for each tissue type. The leftmost column in each group of five images shows the tissue core from a tissue microarray. The middle column shows two images: a small field of view (top) and a zoomed-in view of the area outlined by a white box in the upper image (bottom), all pre-expansion. The rightmost column in each group shows the same fields of view as in the middle column, but post-expansion after having been processed via the ExPath protocol. Blue, DAPI; green, vimentin; magenta, KRT19. **e**, Comparative imaging of kidney podocyte foot processes in both normal and nephrotic (MCD, minimal change disease) disease states with both electron microscopy and ExPath. Each pair of images shows one electron micrograph (left) and one ExPath image (right) from the same subject. The inset in each image shows a zoomed-in view of the region outlined by the box in the main image. Gray, DAPI; blue, collagen IV; green, vimentin; magenta, ACTN4. Panels **d** and **e** reproduced with permission from ref. [12], Springer Nature. Scale bars, 1 μm (**e**, main images (physical size post-expansion, 4.3 μm)), 2 μm (**a**), 10 μm (**b** (physical size post-expansion, 38 μm)), 50 μm (**c**), 200 μm (**d**, tissue core), or 200 nm (**e**, insets). Yellow scale bars in **d** have the same biological scale as the paired white scale bars: top images, 10–12.5 μm; bottom images, 2.5–3.1 μm; physical sizes post-expansion, top images, 50 μm; bottom images, 12.5 μm.

brain synaptic connections and nuclear-cytoskeletal organization[18], imaging of glial and gap junction organization in human brain tissue from subjects with epilepsy[27], and imaging of synaptic proteins to characterize novel connections in mouse striatal brain circuitry (Fig. 2c)[28], among many other biological investigations published at the time of this review's acceptance[29–43].

Another independent attempt at creating a fluorescent protein-retention form of ExM resulted in the protocol ePACT. This approach, in contrast to the other methods described in this section, does not use an explicit protein-anchoring chemical, and uses the milder enzyme collagenase for mechanical homogenization rather than proteinase K[44]. Although ePACT resulted in approximately fourfold expansion of Thy1–YFP+ brain tissue, with YFP fluorescence visible, the authors[44] noted that this was accompanied by tissue destruction, including the compromising of fine processes. In comparison to the other procedures discussed in this section, it is possible that ePACT encounters these difficulties because of its lack of protein-anchoring treatment and the incomplete mechanical homogenization caused by the gentler protease.

In a second style of proExM, endogenous proteins are directly anchored to the polymer hydrogel via AcX and then stained with antibodies post-expansion[9]. In order for epitopes to be retained,

the mechanical homogenization step does not involve protease digestion, but rather proceeds via a gentler homogenization protocol, such as treatment with a high-temperature detergent solution. Use of a gentler protease, such as LysC, which cuts proteins at lysines and thus yields protein fragments that can be of sufficient size to retain epitopes for antibody binding, can also work. After mechanical homogenization and expansion, the specimen can be stained with standard antibodies to allow imaging of proteins with nanoscale resolution (Fig. 3a). In our hands, this protocol worked for many, but not all, antibodies tried, perhaps because epitopes were sometimes lost during heat treatment or during LysC cleavage; this protocol also sometimes led to discontinuities in processes and white matter tracts.

The magnified analysis of the proteome (MAP) protocol[14], developed independently and in parallel to proExM, also allows for the retention and staining of epitopes after expansion, using somewhat different fixation, polymerization, and homogenization steps. In MAP, the expansion of gel-retained proteins away from each other is facilitated by reduction of the amount of cross-linking between proteins during formaldehyde fixation. This is achieved through the addition of acrylamide during fixation, which reacts to formaldehyde bound to proteins and prevents protein–protein cross-linking.
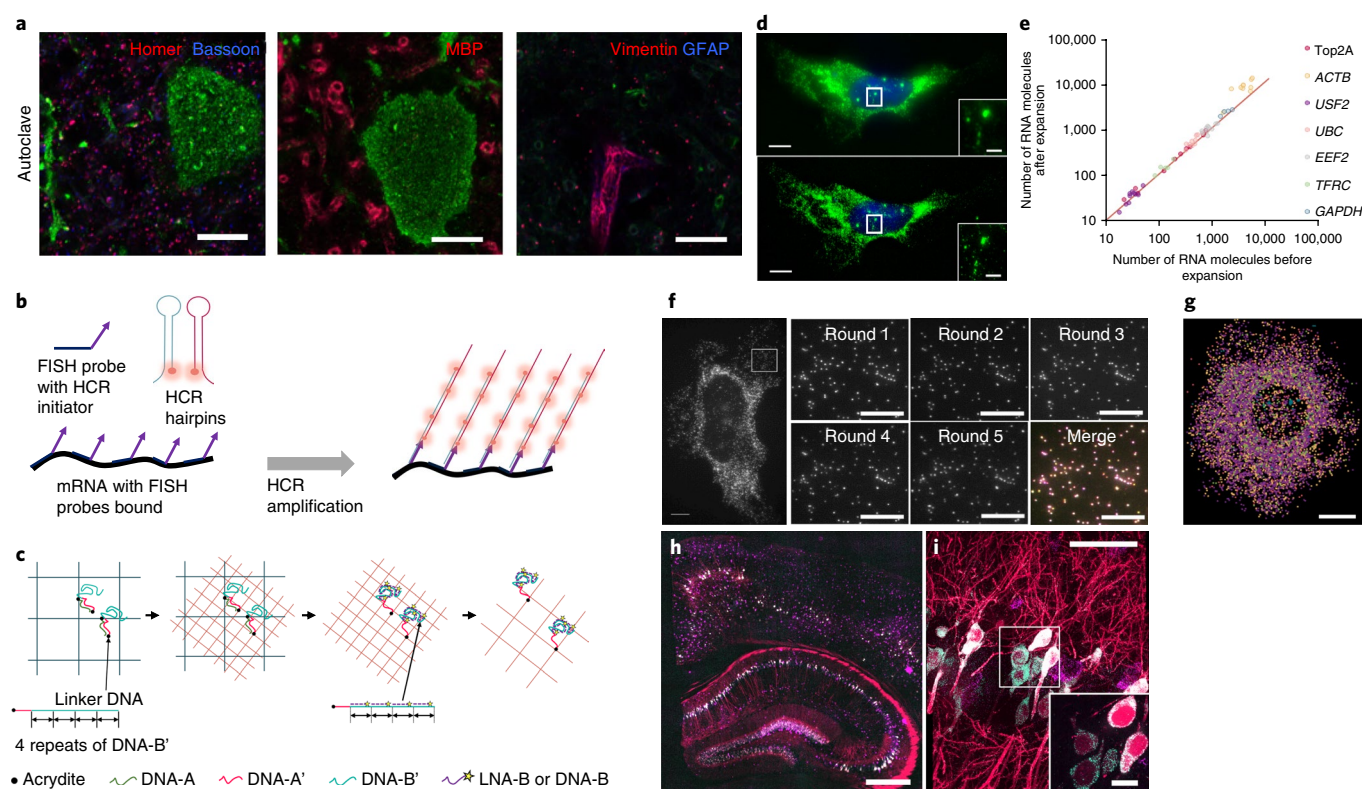
Fig. 3 | ExM decrowds biomolecules, facilitating post-expansion staining, signal amplification, and multiplexed readout. a, Post-expansion antibody staining of protein targets in Thy1–YFP⁺ mouse brain tissue via a variant of proExM that uses high-temperature detergent-based (i.e., epitope-sparing) mechanical homogenization. Images show post-expansion staining with YFP (green), Bassoon (blue), and Homer (magenta) (left); YFP (green) and myelin basic protein (MBP; magenta) (middle); and YFP (green), vimentin (magenta), and glial fibrillar acidic protein (GFAP; blue) (right). Adapted with permission from ref. [9], Springer Nature. **b**, Schematic for HCR-mediated signal amplification. **c**, Schematic showing locked nucleic acid (LNA) and DNA-based signal amplification for iExM. Adapted with permission from ref. [11], Springer Nature. **d**, Top, pre-expansion smFISH image of *ACTB* RNA in a cultured HeLa cell. The inset shows a zoomed-in view of the region outlined by a white box in the main image, highlighting *ACTB* transcription sites in the nucleus. Bottom, as in the top image, but with ExFISH. **e**, smFISH counts of RNA abundance for seven different transcripts before versus after expansion (*n* = 59 cells; each symbol represents one cell). **f**, Left, wide-field fluorescence image of ExFISH targeting *GAPDH* RNA in a cultured HeLa cell. Right, magnified views of the boxed region in the image on the left, representing five repeated cycles of staining and probe removal, as well as an overlay (Merge) of the five images (each with a different color: red, green, blue, magenta, or yellow) showing colocalization. **g**, Composite wide-field image showing ExFISH with serially delivered probes against six RNA targets in a cultured HeLa cell (*NEAT1*, blue; *EEF2*, orange; *GAPDH*, yellow; *ACTB*, purple; *UBC*, green; *USF2*, light blue). **h**, ExFISH post-expansion wide-field fluorescence image of a Thy1–YFP⁺ brain slice showing YFP protein (magenta), *YFP* mRNA (cyan), and *GAD1* mRNA (purple). **i**, Confocal image of mouse hippocampal tissue from **h**, showing single RNA puncta. Inset, one plane of the boxed region in the main image (magenta, YFP protein; cyan, *YFP* mRNA; purple, *GAD1* mRNA). Panels **b** and **d–i** adapted with permission from ref. [10], Springer Nature. Scale bars, 2 µm (**d**, insets (physical size post expansion, 6.6 µm)), 3 µm (**f**, right (10 µm)), 5 µm (**a** (~21 µm)), 6.6 µm (**f**, left (20 µm); **g** (20 µm)), 10 µm (**d** (33 µm); **i**, inset (29 µm)), 50 µm (**i** (145 µm)), or 500 µm (**h** (1,450 µm)).

An open question is how this reduction in cross-linking degree affects nanoscale ultrastructure-level organization. The bound acrylamide also serves to equip proteins with a gel anchorable moiety, as acrylamide can participate in free-radical polymerization just as acrylate does (and indeed, it was the original monomer used in the Hausen–Dreyer protocol[7]). After immersion of the specimen in a mixture of sodium acrylate and acrylamide, and formation of the resulting interpenetrating gel throughout the specimen, incubation in a high-temperature detergent solution causes denaturation of proteins and allows for separation and expansion upon immersion of the specimen in water. Finally, epitopes are labeled via immunostaining after expansion. MAP was initially demonstrated on multiple organs, including heart, lung, liver, kidney, and brain, as well as on cerebral organoids. Post-expansion staining with MAP was demonstrated to work with >80% of the >100 antibodies tested, including antibodies to microtubules, neurofilaments, and a diversity of membrane, cytoplasmic, nuclear, and synaptic proteins[14]. MAP also allows for multiplexed antibody staining by the iterative

staining and removal of antibodies; destaining involves immersion in a high-temperature denaturation solution. Whereas other proExM variants have focused on application to previously fixed tissue sections to facilitate diffusion of reagents into specimens, MAP achieves whole-organ expansion by delivering the necessary reagents (including fixatives) via transcardial perfusion and applying longer incubation times—an approach that potentially could be extended to other ExM methods. At the time of this paper's acceptance, MAP had been used to visualize the glomerular filtration barrier of the kidney in rodents[45].

It is essential to validate the performance of antibodies in order to achieve the highest-fidelity staining possible for post-expansion antibody administration. The use of other tags, such as Snap, Clip, and Halo tags, or the use of nanobodies may also improve the resolution enabled by proExM protocols even further, owing to their smaller size. Recent advancement in multiplexed stimulated Raman scattering has yielded sets of dyes that can be imaged a dozen or more at a time, and thus could also be adapted for multiplexed

imaging of a large number of biomolecules simultaneously in a single ExM sample[46,47]. Another area of future innovation is to rethink microscopy hardware so that the largest volumes possible can be imaged, taking advantage of the fact that expansion protocols can improve resolution in a way that is complementary and orthogonal to traditional microscope design. ProExM-like protocols result in specimens that can be imaged on many conventional microscopes, including the confocal microscopes and epifluorescent microscopes ubiquitous in biology and medicine. For general morphological visualization of cells and tissues, it is possible to expand samples with a proExM-like protocol and then image the resulting expanded samples via bright-field or phase-contrast microscopy to determine the location and organization of membranes and organelles[9]. Such a strategy has been used, for example, to visualize tunneling nanotubes between cultured epithelial cells, which can be exploited by the influenza virus to help it spread from cell to cell and potentially evade the immune system[48]. An exciting possibility just beginning to be explored is that post-expansion staining of specimens may allow for proteins to be decrowded by the expansion process, thereby improving the accessibility and density of staining for proteins even within a dense multicomponent complex.

Samples expanded with proExM have also been imaged with super-resolution microscopes for added resolution beyond what is achievable with conventional microscopes. The use of proExM-anchorable fluorescent proteins makes super-resolution photo-activated localization microscopy possible with expanded cells, potentially enabling very high-resolution imaging; the basic concept has been demonstrated with cultured cells expressing histone H3.3–Dendra2, but the fundamental resolution supported by this methodology has not been fully validated[9]. Other studies have applied super-resolution structured illumination microscopy[36,40] or stimulated emission depletion microscopy[43,45,49] to samples (including microbes, cultured cells, mammalian tissues, and *Drosophila* tissues) expanded with proExM-like protocols. Finally, one group of researchers used the original ExM protocol on samples that they subsequently imaged with inexpensive modified webcams, and found that the resolution improvement enabled by ExM compensated for the poorer resolution of the low-cost microscopy hardware, thus potentially allowing for less expensive biological and medical imaging[24].

Expansion pathology. ExPath is a variant of the pre-expansion antibody-administration proExM protocol optimized for tissue specimens common in human clinical and pathological settings[12]. Formalin-fixed paraffin-embedded, hematoxylin and eosin (H&E)-stained, and fresh-frozen thin-sliced specimens can be preprocessed for use in the proExM pipeline. ExPath starts with a series of steps that make clinically prepared tissues compatible with proExM, such as xylene removal of any paraffin and antigen retrieval in hot sodium citrate. The form of proExM that follows has increased levels of EDTA, which improves tissue digestion in clinical specimens that are sometimes very heavily fixed owing to long exposure to formalin. H&E stains are removed during this processing. For fresh-frozen sections (e.g., acetone-fixed), one reduces the amount of AcX to avoid over-anchoring of specimens, because there are more free amines available in such specimens to bind anchors owing to the lack of aldehyde fixatives occupying amines. The ExPath protocol has been applied to human skin, lung, liver, breast, prostate, pancreas, ovary, kidney, and other tissues (Fig. 2d) preserved via a variety of strategies.

ExPath is compatible with antibody staining, as demonstrated by labeling of many different markers (vimentin, keratin, etc.) in a diversity of tissues, as well as post-expansion DNA FISH against genes (as demonstrated by labeling of Her2 in Her2⁻ and Her2⁺ breast cancer samples from human patients). ExPath reduces autofluorescence by up to an order of magnitude by diluting or eliminating

contributors to autofluorescence while preserving information covalently anchored to the polymer. We demonstrated that ExPath could resolve structures in human specimens that traditionally require electron microscopy imaging for diagnosis, such as podocyte foot processes that are effaced in people with nephrotic kidney diseases (Fig. 2e). Although electron microscopy has superior resolution compared with that of current expansion microscopy protocols, the processing time of ExPath is substantially shorter than that for electron microscopy, and the skills and equipment needed for ExPath are much less demanding compared with those required for electron microscopy. Using ExPath, we were able to greatly improve the performance of a machine learning diagnosis classifier on human breast biopsies. This is an exciting development because agreement between pathologists can be as low as 50% (ref. [50]) on such early breast lesions. These initial clinical studies were small, so future studies involving large numbers of patients will be essential in order for the potential value of ExPath in the clinic to be fully understood.

ExFISH: nanoscale imaging of RNA with expansion microscopy. One powerful attribute of ExM is that it is compatible with the visualization of new molecule classes and the incorporation of new amplification and analysis chemistries (Fig. 3b,c). For example, RNA molecules can be anchored to the swellable polymer by the molecule LabelX, a reagent formed from the reaction of two commercially available reagents[10]. LabelX possesses an alkylating group that reacts primarily to guanine bases in RNA and DNA, as well as a carbon–carbon bond that can be incorporated into the gel. Thus, specimens treated with LabelX can be expanded in an even way. The ability to stain RNA after expansion opens the door to the use of various FISH strategies to interrogate RNA location and identity; we call this suite of technologies ExFISH. We have shown that standard single-molecule FISH (smFISH) can be applied to cultured cells after expansion, thus allowing for imaging of the nanoscale organization of RNA molecules such as long noncoding RNAs (Fig. 1g). The ability of expansion to decrowd RNA molecules improves the quantification of RNA abundance (Fig. 3d,e). Furthermore, expansion supports multiplexed smFISH by allowing for the efficient delivery and removal of probes, thereby making it possible to read out the identity and location of multiple RNA molecules over time (Fig. 3f,g). Another group developed a simple method for visualization of RNAs that involves the application of gel-anchorable fluorescent FISH probes before expansion; the probes are then anchored to the polymer and expanded away from each other[16]. This approach yielded an improved signal-to-noise ratio and more accurate RNA counts than obtained with samples in the unexpanded state[16]. This method does not directly retain RNAs themselves; rather, it retains only the probes applied, and so should be used only when the goal is to image specific transcripts post-expansion, as it will not be possible to wash probes in or out post-expansion.

We anticipate the use of ExFISH with a diversity of signal-amplification strategies to enable better imaging of single RNA molecules in large, intact tissues. Signal-amplification techniques such as hybridization chain reaction (HCR)[51–53] and rolling circle amplification[54,55] produce bright signals by forming large assemblies of fluorophores, which can be easily detected. ExM invites the use of such techniques by creating room for such large assemblies of fluorophores. For instance, we used HCR with ExFISH (Fig. 3b), which allowed for single-molecule-resolution visualization of RNA with nanoscale precision in thick brain tissues (Fig. 3h,i). HCR-ExFISH allows the super-resolved localization of RNA molecules in small compartments, such as neural synapses, while making it possible to image them over large regions of tissue. HCR has also been used to amplify the fluorescence connected to an antibody, thereby enabling protein visualization with a three-orders-of-magnitude boost in

brightness compared with that achieved with conventional antibody staining[53]. Future investigations of how ExFISH protocols could be used for visualization of the 3D configuration of the genome will be of great interest in the probing of epigenetic states, chromatin conformation, and other important determinants of cell fate, function, and health.

Iterative expansion microscopy. In iExM, a specimen is expanded (Fig. 1b), a second swellable gel is synthesized in the space opened up by the first expansion, and the sample is expanded again[11]. The gel synthesized for the first expansion step is made with a chemically cleavable cross-linker, which is cleaved after the second gel is made, thus allowing for further expansion. Biomolecules or labels must also be transferred from the first gel to the second gel to ensure that no information is lost. One way to do this is to initially stain samples with antibodies bearing oligonucleotide barcodes, which are chemically anchored to the first-round expansion polymer. After the first round of expansion, complementary oligonucleotide strands are added, which hybridize to the gel-anchored initial barcodes. These complementary strands are then chemically anchored to the second-round expansion gel and further expanded away from each other. These strands can then be labeled with further hybridizing probes bearing fluorophores (Fig. 3c), which allows for amplification that is greatly helpful given the ~10,000× volumetric dilution of biomolecules or labels relative to the starting condition.

The resolution offered by iExM is comparable to the resolution of the best super-resolution methods that have been applied to cells and tissues (Supplementary Table 1), and thus permits powerful 3D imaging with nanoscale precision in thick specimens on conventional microscopes. The ~25-nm resolution possible with iExM can resolve pre- and postsynaptic proteins such as neurotransmitter receptors and scaffolding proteins within synapses (Fig. 4d,e). Of particular interest is the idea that iExM may allow detailed reconstruction of dense brain circuitry (a theoretical study of this possibility is presented in ref. [56]). Although the spatial resolution of iExM does not yet approach that of electron microscopy, the inherent multicolor nature of optical microscopy can allow multiple kinds of tags, each labeled with different colors, to be used in an intact-tissue nanoscopy context. Thus information represented by one color could, if insufficient for tracing of a neural circuit, be error-corrected by the information represented by a second color[56]. Preliminary studies using Brainbow-labeled mouse cortex suggest that iExM can support the visualization of spines and other compartments along neural processes over extended 3D volumes (Fig. 4a–c).

Can such resolutions be achieved in a single expansion step? Reduction of the cross-linker concentration results in far greater gel expansion factors, but also greater gel fragility[5]. A recently published protocol that uses the additional monomer N,N-dimethylacrylamide acid during the polymerization step presented an ~10× linear expansion[15]. In this method, termed X10 microscopy, N,N-dimethylacrylamide acid serves simultaneously as a monomer and as a cross-linker, replacing the commonly used cross-linker N,N′-methylenebisacrylamide. This modification of the gel chemistry allows the hydrogel to swell up to tenfold in a single expansion step, yielding a resolution of ~25 nm. X10 was demonstrated to work in both cultured cells and mouse brain tissue. Isotropy measurements in cultured cells showed distortion levels similar to those observed with other ExM variants. X10 requires strong protease digestion for mechanical homogenization, which results in the loss of fluorescent protein markers. The authors mitigated this issue by applying fluorescently labeled antibodies to fluorescent protein targets. Like other ExM protocols, X10 will benefit from future validation and optimization; for example, the authors noted that their attempt to expand mouse spleen tissue with X10 resulted in fragmentation, which suggests that for tough tissues, further refinement will be beneficial[15].
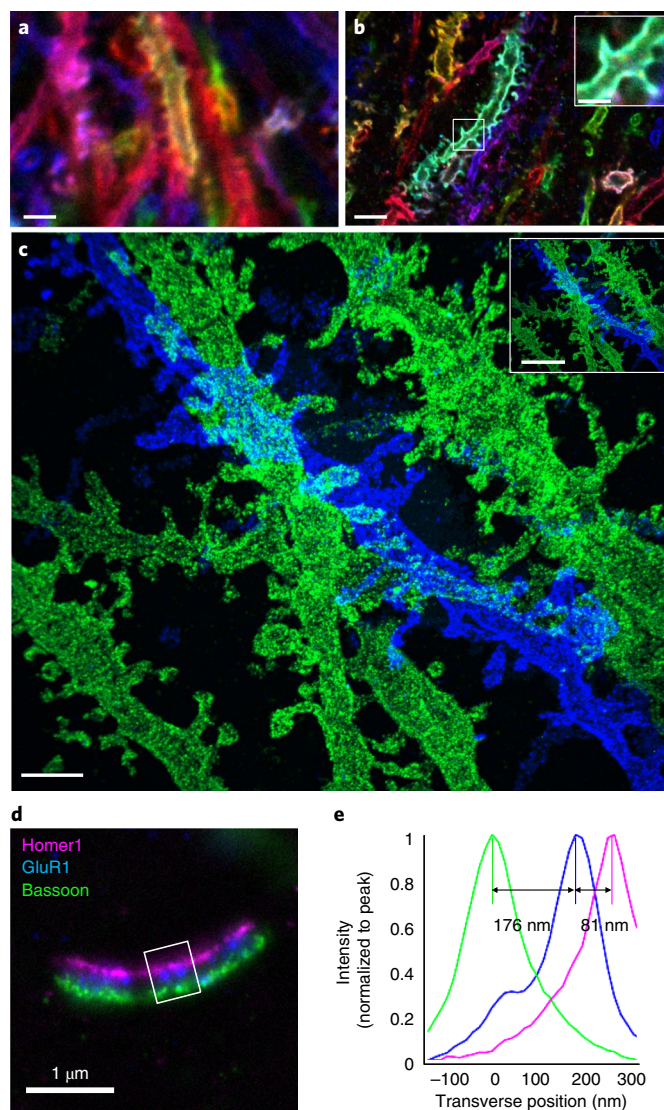

Fig. 4 | Results of 25-nm-resolution imaging of neural circuitry and synapses with iExM. a, Confocal image of immunostained neurons in mouse hippocampus expressing Brainbow3.0, imaged without expansion. Blue, EYFP; red, TagBFP; green, mTFP. **b,** As in **a**, but imaged after 4.5× expansion via proExM; inset shows a magnified image of the boxed region in the main image. **c,** Confocal image (maximum intensity projection) of an iExM (~20×)-expanded specimen of mouse hippocampus immunolabeled with EYFP (blue) and mCherry (green). Inset shows a demagnified view of **c** with the scale bar set to indicate the same distance as the scale bars in **a** and **b**. Panels **a**–**c** reproduced with permission from ref. [11], Springer Nature. **d,** Wide-field image of a synapse from a field of cultured hippocampal neurons immunostained for Homer1 (magenta), glutamate receptor 1 (GluR1; blue), and Bassoon (green). **e,** Transverse profile of the three proteins imaged in **d** (representing the boxed region) after normalization to the peak (Homer1 in magenta, GluR1 in blue, Bassoon in green). Scale bars, 3 μm (**a,b,c** (inset); physical size post-expansion, 14 μm (**b**) or 60 μm (**c,** inset)) or 1 μm (**b** (inset),**c,d**; physical size post-expansion, 4.5 μm (**b,** inset), 20 μm (**c**), or 13 μm (**d**)).

One interesting question is how different ExM protocols might be combined. For example, can the iExM protocol be combined with ExFISH, so that ultraprecise volumetric visualization of RNAs in extended intact tissues is possible? Can iExM be combined with the post-expansion-antibody-administration forms of proExM and MAP, so that epitopes can be decrowded for denser and

higher-resolution antibody staining? And can the procedure be automated, so that extremely high-throughput processing of cells and tissues is possible? These questions represent opportunities for biotechnological innovation in the next few years, and in turn for downstream biological and medical discovery.

Outlook

We have tried to document the status of specific ExM protocols, as well as where they are headed. We now offer some general comments on the state and future of the entire tool suite, in terms of fundamental performance and limitations. Compared with conventional super-resolution microscopy (SRM) methods, ExM offers numerous technical advantages, such as the ability to perform 3D nanoscale imaging of thick fixed specimens, as well as speed and ease of use (Supplementary Table 1, Supplementary Note 1). In addition, ExM yields transparent samples as a byproduct of its physical mechanism. In contrast to other clearing techniques, ExM clears samples via the expansion process, which results in a hydrogel composed mostly of water (Supplementary Table 2, Supplementary Note 2). The clearest disadvantage of ExM is its incompatibility with live samples. In contrast to SRM methods, ExM poses unique considerations owing to its physical mechanism. The expansion achieved is designed to be isotropic, and measurements of isotropy with different ExM methods have shown that distortions arising from the expansion process are minimal, but not zero (Supplementary Table 1, Supplementary Note 1).

Although iExM currently offers 3D nanoscale imaging in tissues with resolution comparable to that of the best-performing SRM techniques, it might be possible to achieve even higher levels of expansion and resolution by improving polymer composition and processing protocols. Already a proof-of-concept triple expansion has been demonstrated, resulting in ~53× linear expansion, although the resolution was not validated[11]. This might actually exceed the resolution of existing SRM technologies if antibodies or other labels are delivered post-expansion, thus reducing the resolution error introduced by the nonzero size of the tags that comes into play when the tags are delivered to a nonexpanded tissue.

Another area of future interest is the combination of multiple protocols. A unified protocol that enabled the visualization of DNA, RNA, proteins, and lipids could reveal the organization of complexes of multiple kinds of biomolecules. Already the combined use of protein-anchoring AcX and RNA-labeling LabelX has been used to visualize fluorescent proteins and FISH-labeled RNAs in the same sample[10], and the ExPath protocol has been used for DNA FISH in concert with antibody labeling of proteins in the same sample[12]. The combination of multimodal anchoring and labeling strategies with iExM is also an exciting future direction, and could potentially allow many biomolecules to be visualized in a single sample with extremely high resolution.

The aqueous nature of expanded specimens and the decrowding of biomolecules may open the door for highly multiplexed readout of molecular information with nanoscale precision. ExFISH has already been used for serial staining with multiple FISH probes for multiplexed imaging of different transcripts after RNA anchoring and expansion[10]. It may be possible to implement in intact tissues the use of barcoded, combinatorial RNA-FISH multiplexing approaches[57,58], such as MERFISH[59–61] and seqFISH[62], in which coded FISH probes are administered serially to yield the location of exponentially increasing numbers of transcripts over many cycles of hybridization. The ability to follow individual transcripts over many rounds of hybridization would be facilitated by the decrowding of transcripts. Indeed, ExM has been used with MERFISH to visualize, with 10× higher density, members of an ~130-RNA library with nearly 100% detection efficiency in cultured cells[61]. The covalent anchoring of RNA to the polymer may also help support controlled enzymatic reactions such as fluorescent in situ sequencing

of RNA[54,55]. Such approaches would yield transcriptome data in conjunction with cell morphology, protein locations, and other biomolecular information, with nanoscale precision.

Such techniques could also be used to identify any biomolecular labels conjugated to oligonucleotide barcodes that are retained within the gel (as seen, for example, with the use of DNA-PAINT-style probes[63]). For instance, it may be possible to deliver antibodies to various targets, each bearing a unique oligonucleotide tag that can be read out after expansion via multiplexed FISH or in situ sequencing, thus providing location and identity information for very large numbers of proteins. This scheme could be extended to label any biomolecule with an oligonucleotide barcode that can be identified after expansion, thereby enabling the nanoscale mapping of biomolecules throughout specimens in a highly multiplexed fashion.

References

1. Dunn, R. C. Near-field scanning optical microscopy. *Chem. Rev.* **99**, 2891–2928 (1999).
2. Dürig, U., Pohl, D. W. & Rohner, F. Near-field optical-scanning microscopy. *J. Appl. Phys.* **59**, 3318–3327 (1986).
3. Hell, S.W. Far-field optical nanoscopy. In *Proc. 2010 23rd Annual Meeting of the IEEE Photonics Society* (eds Jagadish, C. et al.) 3–4 (IEEE, New York, 2010).
4. Huang, B., Bates, M. & Zhuang, X. Super-resolution fluorescence microscopy. *Annu. Rev. Biochem.* **78**, 993–1016 (2009).
5. Chen, F., Tillberg, P. W. & Boyden, E. S. Expansion microscopy. *Science* **347**, 543–548 (2015).
6. Tanaka, T. et al. Phase transitions in ionic gels. *Phys. Rev. Lett.* **45**, 1636–1639 (1980).
7. Hausen, P. & Dreyer, C. The use of polyacrylamide as an embedding medium for immunohistochemical studies of embryonic tissues. *Stain Technol.* **56**, 287–293 (1981).
8. Cohen, Y., Ramon, O., Kopelman, I. J. & Mizrahi, S. Characterization of inhomogeneous polyacrylamide hydrogels. *J. Polym. Sci. B Polym. Phys.* **30**, 1055–1067 (1992).
9. Tillberg, P. W. et al. Protein-retention expansion microscopy of cells and tissues labeled using standard fluorescent proteins and antibodies. *Nat. Biotechnol.* **34**, 987–992 (2016).
10. Chen, F. et al. Nanoscale imaging of RNA with expansion microscopy. *Nat. Methods* **13**, 679–684 (2016).
11. Chang, J.-B. et al. Iterative expansion microscopy. *Nat. Methods* **14**, 593–599 (2017).
12. Zhao, Y. et al. Nanoscale imaging of clinical specimens using pathology-optimized expansion microscopy. *Nat. Biotechnol.* **35**, 757–764 (2017).
13. Chozinski, T. J. et al. Expansion microscopy with conventional antibodies and fluorescent proteins. *Nat. Methods* **13**, 485–488 (2016).
14. Ku, T. et al. Multiplexed and scalable super-resolution imaging of three-dimensional protein localization in size-adjustable tissues. *Nat. Biotechnol.* **34**, 973–981 (2016).
15. Truckenbrodt, S. et al. X10 expansion microscopy enables 25-nm resolution on conventional microscopes. *EMBO Rep.* **19**, e45836 (2018).
16. Tsanov, N. et al. smiFISH and FISH-quant—a flexible single RNA detection approach with super-resolution capability. *Nucleic Acids Res.* **44**, e165 (2016).
17. Asano, S. M. et al. Expansion microscopy: protocols for imaging proteins and RNA in cells and tissues. *Curr. Protoc. Cell Biol.* **80**, e56 (2018).
18. Freifeld, L. et al. Expansion microscopy of zebrafish for neuroscience and developmental biology studies. *Proc. Natl Acad. Sci. USA* **114**, E10799–E10808 (2017).
19. Migliori, B. et al. Light sheet theta microscopy for rapid high-resolution imaging of large biological samples. *BMC Biol.* **16**, 57 (2018).
20. Hama, H. et al. Scale: a chemical approach for fluorescence imaging and reconstruction of transparent mouse brain. *Nat. Neurosci.* **14**, 1481–1488 (2011).
21. Susaki, E. A. et al. Whole-brain imaging with single-cell resolution using chemical cocktails and computational analysis. *Cell* **157**, 726–739 (2014).
22. Chung, K. et al. Structural and molecular interrogation of intact biological systems. *Nature* **497**, 332–337 (2013).
23. Murakami, T. C. et al. A three-dimensional single-cell-resolution whole-brain atlas using CUBIC-X expansion microscopy and tissue clearing. *Nat. Neurosci.* **21**, 625–637 (2018).
24. Zhang, Y. S. et al. Hybrid microscopy: enabling inexpensive high-performance imaging through combined physical and optical magnifications. *Sci. Rep.* **6**, 22691 (2016).

25. Aoki, T., Tsuchida, S., Yahara, T. & Hamaue, N. Novel assays for proteases using green fluorescent protein-tagged substrate immobilized on a membrane disk. *Anal. Biochem.* **378**, 132–137 (2008).

26. Nicholls, S. B. & Hardy, J. A. Structural basis of fluorescence quenching in caspase activatable-GFP. *Protein Sci.* **22**, 247–257 (2013).

27. Deshpande, T. et al. Subcellular reorganization and altered phosphorylation of the astrocytic gap junction protein connexin43 in human and experimental temporal lobe epilepsy. *Glia* **65**, 1809–1820 (2017).

28. Crittenden, J. R. et al. Striosome-dendron bouquets highlight a unique striatonigral circuit targeting dopamine-containing neurons. *Proc. Natl Acad. Sci. USA* **113**, 11318–11323 (2016).

29. Decarreau, J. et al. The tetrameric kinesin Kif25 suppresses pre-mitotic centrosome separation to establish proper spindle orientation. *Nat. Cell Biol.* **19**, 384–390 (2017).

30. Suofu, Y. et al. Dual role of mitochondria in producing melatonin and driving GPCR signaling to block cytochrome c release. *Proc. Natl Acad. Sci. USA* **114**, E7997–E8006 (2017).

31. Wang, Y. et al. Combined expansion microscopy with structured illumination microscopy for analyzing protein complexes. *Nat. Protoc.* **13**, 1869–1895 (2018).

32. Orth, A. et al. Super-multiplexed fluorescence microscopy via photostability contrast. *Biomed. Opt. Express* **9**, 2943–2954 (2018).

33. Chozinski, T. J. et al. Volumetric, nanoscale optical imaging of mouse and human kidney via expansion microscopy. *Sci. Rep.* **8**, 10396 (2018).

34. Tsai, A. et al. Nuclear microenvironments modulate transcription from low-affinity enhancers. *eLife* **6**, e28975 (2017).

35. Jiang, N. et al. Superresolution imaging of *Drosophila* tissues using expansion microscopy. *Mol. Biol. Cell* **29**, 1413–1421 (2018).

36. Cahoon, C. K. et al. Superresolution expansion microscopy reveals the three-dimensional organization of the *Drosophila* synaptonemal complex. *Proc. Natl Acad. Sci. USA* **114**, E6857–E6866 (2017).

37. Sümbül, U. et al. Automated scalable segmentation of neurons from multispectral images. In *Advances in Neural Information Processing Systems 29* (eds Lee, D. D. et al.) 1912–1920 (NIPS Foundation, La Jolla, CA, 2016).

38. Mosca, T. J., Luginbuhl, D. J., Wang, I. E. & Luo, L. Presynaptic LRP4 promotes synapse number and function of excitatory CNS neurons. *eLife* **6**, 1–29 (2017).

39. Wang, I. E., Lapan, S. W., Scimone, M. L., Clandinin, T. R. & Reddien, P. W. Hedgehog signaling regulates gene expression in planarian glia. *eLife* **5**, e16996 (2016).

40. Halpern, A. R., Alas, G. C. M., Chozinski, T. J., Paredez, A. R. & Vaughan, J. C. Hybrid structured illumination expansion microscopy reveals microbial cytoskeleton organization. *ACS Nano* **11**, 12677–12686 (2017).

41. Artur, C. G. et al. Plasmonic nanoparticle-based expansion microscopy with surface-enhanced Raman and dark-field spectroscopic imaging. *Biomed. Opt. Express* **9**, 603–615 (2018).

42. Villaseñor, R., Schilling, M., Sundaresan, J., Lutz, Y. & Collin, L. Sorting tubules regulate blood-brain barrier transcytosis. *Cell Rep.* **21**, 3256–3270 (2017).

43. Li, R., Chen, X., Lin, Z., Wang, Y. & Sun, Y. Expansion enhanced nanoscopy. *Nanoscale* **10**, 17552–17556 (2018).

44. Treweek, J. B. et al. Whole-body tissue stabilization and selective extractions via tissue-hydrogel hybrids for high-resolution intact circuit mapping and phenotyping. *Nat. Protoc.* **10**, 1860–1896 (2015).

45. Unnersjö-Jess, D. et al. Confocal super-resolution imaging of the glomerular filtration barrier enabled by tissue expansion. *Kidney Int.* **93**, 1008–1013 (2018).

46. Wei, L. et al. Super-multiplex vibrational imaging. *Nature* **544**, 465–470 (2017).

47. Hu, F. et al. Supermultiplexed optical imaging and barcoding with engineered polyynes. *Nat. Methods* **15**, 194–200 (2018).

48. Kumar, A. et al. Influenza virus exploits tunneling nanotubes for cell-to-cell spread. *Sci. Rep.* **7**, 40360 (2017).

49. Gao, M. et al. Expansion stimulated emission depletion microscopy (ExSTED). *ACS Nano* **12**, 4178–4185 (2018).

50. Elmore, J. G. et al. Diagnostic concordance among pathologists interpreting breast biopsy specimens. *J. Am. Med. Assoc.* **313**, 1122–1132 (2015).

51. Choi, H. M. T. et al. Programmable in situ amplification for multiplexed imaging of mRNA expression. *Nat. Biotechnol.* **28**, 1208–1212 (2010).

52. Choi, H. M. T., Beck, V. A. & Pierce, N. A. Next-generation in situ hybridization chain reaction: higher gain, lower cost, greater durability. *ACS Nano* **8**, 4284–4294 (2014).

53. Lin, R. et al. A hybridization-chain-reaction-based method for amplifying immunosignals. *Nat. Methods* **15**, 275–278 (2018).

54. Lee, J. H. et al. Highly multiplexed subcellular RNA sequencing in situ. *Science* **343**, 1360–1363 (2014).

55. Ke, R. et al. In situ sequencing for RNA analysis in preserved tissue and cells. *Nat. Methods* **10**, 857–860 (2013).

56. Yoon, Y.-G. et al. Feasibility of 3D reconstruction of neural morphology using expansion microscopy and barcode-guided agglomeration. *Front. Comput. Neurosci.* **11**, 97 (2017).

57. Lubeck, E. & Cai, L. Single-cell systems biology by super-resolution imaging and combinatorial labeling. *Nat. Methods* **9**, 743–748 (2012).

58. Lubeck, E., Coskun, A. F., Zhiyentayev, T., Ahmad, M. & Cai, L. Single-cell in situ RNA profiling by sequential hybridization. *Nat. Methods* **11**, 360–361 (2014).

59. Chen, K. H., Boettiger, A. N., Moffitt, J. R., Wang, S. & Zhuang, X. Spatially resolved, highly multiplexed RNA profiling in single cells. *Science* **348**, aaa6090 (2015).

60. Moffitt, J. R. et al. High-throughput single-cell gene-expression profiling with multiplexed error-robust fluorescence in situ hybridization. *Proc. Natl Acad. Sci. USA* **113**, 11046–11051 (2016).

61. Wang, G., Moffitt, J. R. & Zhuang, X. Multiplexed imaging of high-density libraries of RNAs with MERFISH and expansion microscopy. *Sci. Rep.* **8**, 4847 (2018).

62. Shah, S., Lubeck, E., Zhou, W. & Cai, L. In situ transcription profiling of single cells reveals spatial organization of cells in the mouse hippocampus. *Neuron* **92**, 342–357 (2016).

63. Wang, Y. et al. Rapid sequential in situ multiplexing with DNA-exchange-imaging in neuronal cells and tissues. *Nano Lett.* **17**, 6131–6139 (2017).

Acknowledgements

Author contributions

A.T.W., Y.Z., and E.S.B. all contributed to the writing of the manuscript and have read and agreed to its content.

Competing interests

E.S.B. is a co-inventor on multiple patents related to ExM and is also a co-founder of a company (http://extbio.com/) commercializing ExM. Y.Z. and A.T.W. are inventors on several inventions related to ExM.

Additional information

Supplementary information is available for this paper at https://doi.org/10.1038/s41592-018-0219-4.

Reprints and permissions information is available at www.nature.com/reprints.

Correspondence should be addressed to E.S.B.

Publisher's note: Springer Nature remains neutral with regard to jurisdictional claims in published maps and institutional affiliations.

Expansion microscopy: principles and uses in biological research

Asmamaw T. Wassie[1,2,3,4,8], Yongxin Zhao[4,5,8] and Edward S. Boyden[1,2,3,4,6,7]*

[1]Department of Brain and Cognitive Sciences, Massachusetts Institute of Technology, Cambridge, MA, USA. [2]Department of Biological Engineering, Massachusetts Institute of Technology, Cambridge, MA, USA. [3]McGovern Institute, Massachusetts Institute of Technology, Cambridge, MA, USA. [4]Media Lab, Massachusetts Institute of Technology, Cambridge, MA, USA. [5]Department of Biological Sciences, Carnegie Mellon University, Pittsburgh, PA, USA. [6]Koch Institute, Massachusetts Institute of Technology, Cambridge, MA, USA. [7]Center for Neurobiological Engineering, Massachusetts Institute of Technology, Cambridge, MA, USA. [8]These authors contributed equally: Asmamaw T. Wassie and Yongxin Zhao. *e-mail: esb@media.mit.edu

Supplementary Table 1 Comparison of ExM and its variants with various super-resolution optical microscopy techniques

Principle	Patterned Illumination		Single Molecule Localization		Physical Magnification		
SRM Technique	STED	SIM	STORM/PALM[a]	DNA PAINT	Pre-Expansion labeling	Post-expansion labeling	iExM
					ExM1.0/proExM/ExPath/	proExM/MAP/ExFISH	
Lateral Resolution[a]	20-60nm[1–4]	~ 100nm[5–7]	20-30nm[8–11]	10-50nm[12–14]	65-75nm[15–17]	65-75nm[15,18], 100nm (ExFISH)[19]	25nm[20]
Axial Resolution[a]	500-700nm[21], 30-50nm (isoSTED)[22,23]	~ 300nm (3D-SIM)[5,6]	50-70nm (3D STORM)[9,10] ~100nm (2D STORM, TIRF)[21] 75nm (BP-FPALM)[24] 15-25nm (iPALM)[11] 20nm (dual objective)[25]	80nm[12]	~ 200nm[15–17]	200nm[15,18], 300nm (ExFISH)[19]	50nm[20]
Depth of Imaging	10-80μm[26,27]	10-20μm[21]	< 10μm[9,21]	10μm[12]	~ 250μm-1mm (limited by working distance and numerical aperture of objective)[15–17]	~250μm-1mm (limited by working distance and numerical aperture of objective)[15,18,19]	~100μm - 500μm (limited by working distance and numerical aperture of objective)[20]
Speed[b]	2D Speed ~ 10^2μm²/s-10^3μm²/s[28–30] 3D Speed ~ 10μm³/s (estimated)[31]	2D Speed ~ 10^3μm²/s (TIRF-SIM)[7] 3D Speed ~ 10^2μm³/s - 10^3μm³/s[32,33]	2D Speed ~ 10^3μm²/s (2D-STORM)[34,35] 3D Speed ~ 10^2μm³/s (estimated)[34]	2D Speed ~1μm²/s-10μm²/s[12–14] 3D Speed ~ 1μm³/s (estimated)[12]	2D Speed ~ 10^4μm²/s-10^5μm²/s (Spinning Disk Confocal)[15–17] 3D Speed ~ 10^4μm³/s (light sheet, estimated)[19]	2D Speed ~ 10^4μm²/s-10^5μm²/s (Spinning Disk Confocal)[15,18,19] 3D Speed ~ 10^4μm³/s (light sheet)[19]	2D Speed ~ 10^3μm²/s-10^4μm²/s (Spinning Disk Confocal)[20] 3D Speed ~ 10^3μm³/s (light sheet, estimated)[19]

Maximum number of colors imaged simultaneously in biological samples	2-3[2,36–38]	4[6]	2-3[39–41]	3[12]	3-4[15–17]	3-4[15,18,19]	3-4[20]
Live Imaging	Yes[28,42]	Yes[7,32,33]	Yes[34,43]	No[12,44]	No[15–17]	No[15,18,19]	No[20]
Probe requirements	Photostable dyes and FPs[4,36,42]	Conventional dyes[6,7]	Photoswitchable dyes and FPs[8,34,45]	Oligonucleotide coupled labels and dyes[12,44,46]	Conventional dyes and fluorescent proteins (except for cyanine family dyes)[15–17]	Conventional dyes[15,18,19]	Conventional dyes (except for cyanine family dyes)[20]
Root Mean Square (RMS) measurement length error due to distortion (as a function of measurement length)	-	-	-	-	1-4% (over 0-2500µm) (ExM 1.0) 1-5% (over 0-100µm) (proExM) 1-3% (over 0-1500µm) (ExPATH)	3-4% (over 0-2000µm) (MAP) <1% (over 0-160µm) (ExFISH)	2.5% (over 0-40µm)

a Resolutions demonstrated in an *in situ* biological context

b Given speeds are for single color.

Supplementary Table 2 Comparison of ExM and its variants with various tissue clearing methods

Mechanism of clearing	Clearing method	Final RI	Time for processing (after fixation)	FP preservation	Demonstrated compatibility with immunostaining
Solvent-based dehydration and RI matching	3DISCO [47]	1.56[47]	Hours-days[47]	Limited, 1-2 days[47]	Yes[47]
	iDISCO [48]	1.56[48]	Days-weeks[48]	Limited, 1-2 days[48]	Yes[48]
Immersion and RI matching in aqueous solution	SeeDB [49]	1.49[49]	Days[49]	Yes[49]	Yes[49]
	TDE [50,51]	1.42-1.45[50,51]	Hours-Days[50,51]	Yes[50,51]	Yes[51]
Hyperhydration	Sca*l*e [52]	1.38[52]	Days-months[52]	Yes[52]	No[52]
	Sca*l*eS[53]	1.44[53]	Days[53]	Yes[53]	Yes[53]
	CUBIC [54]	1.49[54]	Days-weeks[54]	Yes[54]	Yes[54]
	CUBIC-X[55]	1.467[55]	Days-weeks[55]	Yes[55]	No[55]
Hydrogel Embedding, Lipid removal, and RI matching	CLARITY [56]	1.45[56]	Days-weeks[56,57]	Yes[56]	Yes[56]
	PACT, PARS [58,59]	1.38-1.48[58,59]	Days-weeks[58,59]	Yes[58,59]	Yes[58,59]
Dilution caused by expansion, removal of non-anchored biomolecules, RI matching with water immersion lens	ExM: ExM 1.0, proExM, ExFISH, ExPATH, MAP, iExM [15–20,60]	1.33	Days	Yes	Yes

Supplementary Note 1. Comparison between expansion microscopy and other super-resolution imaging techniques

Classical super-resolution microscopy (SRM) techniques achieve high levels of resolution by overcoming Abbe's diffraction limit (on the order of half the wavelength of light) via two general classes of strategy. The first class of strategy uses patterned illumination to manipulate the fluorescence behavior of molecules in a region smaller than the diffraction limit. This way, nearby fluorophores within a diffraction-limited distance can be uniquely identified, thereby achieving subdiffraction-limit resolution. For example, stimulated emission depletion (STED) microscopy[61,62], REversible Saturable Optical Linear Fluorescence Transitions (RESOLFT) technology[63], and super-resolution structured illumination microscopy (SIM)[64,65] belong to this group. The second class of strategy utilizes the photoswitching properties of genetically encoded or small-molecule fluorophores to stochastically enable individual molecules to be visualized at different times, so that each frame contains sparsely distributed, rarely overlapping bright spots representing individual fluorophores, for which the localization can be determined with nanoscale precision by calculation of the centroid of each spot. Assembling these points over time enables reconstruction of the entire image, but now with nanoscale resolution. This second group includes photoactivated localization microscopy (PALM)[45], fluorescence photoactivation localization microscopy (FPALM)[66], stochastic optical reconstruction microscopy (STORM)[67], and DNA points accumulation for imaging in nanoscale topography (DNA PAINT)[44,68]. The first class of strategy presents specialized hardware requirements (e.g., special laser or optical configurations), and while the second class of strategy can take advantage of conventional widefield or TIRF microscopes, one challenge is in achieving high efficacy contrast and switching of single molecules. In addition, these tools can be complex to use, and exhibit shallow depth of imaging capability, and/or slow imaging speed in comparison to standard microscopes. ExM, of course, is a relatively new technology and thus early adopters may need to be adaptable when trying it out for the first time, but protocols are freely available[69] and tutorials explaining how to overcome standard debugging problems (e.g., sample drift during handling, delicacy of expanded samples) have been published[70,71].

In comparison to standard SRM approaches, ExM offers numerous technical advantages – and some disadvantages (**Supplementary Table 1**). ExM does not require any additional hardware beyond what typical labs already have access to. ExM also enables 3D-nanoscale imaging in thick specimens, and over large volumes. Especially with the advent of microscope objectives with long working distances and high numerical aperture (NA), which can support imaging over long axial distances, potentially very large depths (e.g., millimeter to centimeter depth) could be accessed with nanoscale resolution using ExM. In particular, the transparency (**Fig. 1C**) and refractive index homogeneity of ExM-processed samples enables fast 3D imaging microscopy techniques, such as light-sheet microscopy, to be used with ExM to enable fast, 3D, super-resolution imaging. ExM is compatible with a wide range of fluorophores and fluorescent proteins. In terms of lateral and axial resolutions, ExM variants such as ExM1.0, proExM, ExFISH, and ExPath perform better than SIM, while allowing imaging of thick specimens and/or large volumes. iExM achieves resolutions comparable to STED, PALM, and STORM while maintaining the many advantages of ExM described above. A common question is whether

expanding a specimen slows down imaging, because a greater volume must be imaged; all super-resolution methods are slower than their diffraction limited counterparts, but ExM has a "best of both worlds" attribute – it has the voxel sizes of super-resolution microscopy, but the voxel acquisition speeds of fast diffraction limited microscopy. Of course, a clear limitation of ExM is that it is not compatible with live-cell imaging and is unlikely ever to be fully adapted to a general live imaging context.

There are considerations and caveats that are unique to ExM, because of its reliance on physical magnification as opposed to optical magnification. Of course, the expansion of the sample must be isotropic and even, to a level acceptable for the biological or medical question under investigation. Isotropy is typically quantified, when ExM is first applied to a given tissue type, by measuring the distortions incurred during expansion, by aligning and comparing pre- and post-expansion images of the same specimen via a non-rigid registration process. Pre-expansion images are typically taken with a classical super-resolution method, and post-expansion images by a confocal microscope. For the published ExM methods, and across a wide variety of samples, the distortions are ~1-5% of measurement length, over length scales from tens of microns to hundreds of microns (**Supplementary Table 1**). While non-zero, such distortions are acceptable for a wide variety of biological and medical investigations; nevertheless, in the future, new polymer chemistries might reduce the error still further. In addition, some specimens like C. elegans, with its tough cuticle, or bone, may pose special challenges in terms of insuring even expansion, requiring additional technology development and validation beyond existing protocols.

In addition to distortion errors across extended distances, there are nanoscale resolution errors that arise from the gelation and expansion process. We estimated that for iExM, the ExM method with the greatest degree of physical magnification described to date, the resolution error added by gelation and expansion is between 5-10 nm; we estimated this by studying the broadening of the point spread function (PSF), as modeled by the side wall of a microtubule, caused by sample expansion[20]. This level of error is beginning to approach the expected mesh size (i.e., polymer spacing) for polyacrylamide gels (1-2 nm)[72], and it implies an upper limit on the resolution that can be potentially be achieved with the current free radical-synthesized ExM gel chemistry. Of course, higher expansion factors would be required to get the resolution down to this level. And while this value points to a potential error on the length scale of an individual biomolecule, the actual precision in localizing a given biological target would depend on the type of label used. For instance, antibodies applied before expansion could add ~20 nm to the imprecision of localizing individual protein targets, while oligonucleotide tags (as used in iExM) would add another ~ 4-5 nm[20].

In addition, labeling density is an important consideration-- insufficient labeling density causes misrepresentation of the biological structure in question. Though label size and density are issues shared with conventional SRM methods, they could, in principle, be overcome by a unique feature of ExM: the application of tags after expansion, when biomolecular targets have been moved apart from each other. In such a case, positional errors due to the size of labels would be reduced, because the effective tag size would be divided by the expansion factor (e.g.,

post-20x expansion applied antibodies would, in principle, introduce an error of ~20/20 ~ 1 nm). This kind of logic explains why ExM is amenable to signal amplification post-expansion since the effective size of an amplified tag is much lower than its actual size (e.g. with HCR amplification, a 500 nm HCR amplicon created after a 3x ExFISH expansion would have an effective size, in biological terms, of 500 / 3 ~ 150 nm)[19,20]. Of course, the amplification step itself should be as isotropic as possible. But any error in the isotropy of the amplification process will, if performed post-expansion, be divided by the expansion factor. In summary, postponing amplification and other post-labeling analysis steps until after expansion is complete may enhance image quality.

Finally, the resolution of ExM methods have been validated, to date, by studying known biological structures such as microtubules. While this approach works well in contexts where such known structures are present, going forward, ExM would benefit from versatile approaches that allow the measurement of its resolution in any given biological context. Such approaches might include engineered, nanoscale structures like DNA-origami nanorulers[73,74] or artificial protein-complexes[75] that can be added to samples pre-expansion, and imaged after expansion, so that the final structure can be compared to the known ground truth.

Supplementary Note 2. Expansion Microscopy and tissue clearing

ExM achieves tissue clearing as a byproduct of its physical mechanism. This raises the question of how ExM compares to other methods that result in tissue clearing. Biological specimens appear opaque due to an inhomogeneous refractive index (RI) arising from the distribution of the various molecular components of tissues. This inhomogeneity results in non-uniform scattering, which renders the specimen opaque. Furthermore, absorption of light by molecules reduces imaging depth. Tissue clearing techniques work by homogenizing the RI within a specimen so that non-uniform light scattering is minimized[76]. Various techniques clear tissues using various chemical approaches to homogenize RI within specimens (**Supplementary Table 2**). Some of these approaches include solvent-based dehydration and RI matching (3DISCO, BABB, iDISCO)[47,48,77], hyper-hydration based clearing (Sca*l*e, CUBIC)[52,54], RI matching in aqueous solutions (SeeDB)[49], and hydrogel-supported lipid-removal and RI matching (CLARITY, PACT/PARS)[56,59]. The last set of protocols also use hydrogel embedding chemistries related to the Hausen and Dreyer protocol[78], but follow the embedding with removal of the lipids and immersion in compounds that even out refractive index. In comparison, the physical magnification of specimens via ExM homogenizes RI within specimens via dilution of all the polymer-anchored components in water. After expansion, >99% of the volume of the gel is composed of water, which homogenizes the RI of the expanded specimen and matches the RI to that of water (1.33), rendering it transparent. In addition, the loss of non-anchored biomolecules during the expansion process also contributes to the clearing of the specimens by rendering the non-aqueous component more uniform. However, most ExM variants have only been applied to relatively small specimens to date, with the exception of MAP and CUBIC-X, which have been applied to an entire mouse brain[18,55].

References

1.	Donnert, G. *et al.* Macromolecular-scale resolution in biological fluorescence microscopy. *Proc. Natl. Acad. Sci. U. S. A.* **103,** 11440–5 (2006).

2.	Meyer, L. *et al.* Dual-Color STED Microscopy at 30-nm Focal-Plane Resolution. *Small* **4,** 1095–1100 (2008).

3.	WILDANGER, D., MEDDA, R., KASTRUP, L. & HELL, S. W. A compact STED microscope providing 3D nanoscale resolution. *J. Microsc.* **236,** 35–43 (2009).

4.	Willig, K. I., Harke, B., Medda, R. & Hell, S. W. STED microscopy with continuous wave beams. *Nat. Methods* **4,** 915–918 (2007).

5.	Gustafsson, M. G. L. *et al.* Three-dimensional resolution doubling in wide-field fluorescence microscopy by structured illumination. *Biophys. J.* **94,** 4957–70 (2008).

6.	Schermelleh, L. *et al.* Subdiffraction multicolor imaging of the nuclear periphery with 3D structured illumination microscopy. *Science* **320,** 1332–6 (2008).

7.	Kner, P., Chhun, B. B., Griffis, E. R., Winoto, L. & Gustafsson, M. G. L. Super-resolution video microscopy of live cells by structured illumination. *Nat. Methods* **6,** 339–342 (2009).

8.	Heilemann, M. *et al.* Subdiffraction-Resolution Fluorescence Imaging with Conventional Fluorescent Probes. *Angew. Chemie Int. Ed.* **47,** 6172–6176 (2008).

9.	Huang, B., Jones, S. A., Brandenburg, B. & Zhuang, X. Whole-cell 3D STORM reveals interactions between cellular structures with nanometer-scale resolution. *Nat. Methods* **5,** 1047–1052 (2008).

10.	Huang, B., Wang, W., Bates, M. & Zhuang, X. Three-Dimensional Super-Resolution Reconstruction Microscopy. *Science (80-.).* **319,** 810–813 (2008).

11.	Shtengel, G. *et al.* Interferometric fluorescent super-resolution microscopy resolves 3D cellular ultrastructure. *Proc. Natl. Acad. Sci. U. S. A.* **106,** 3125–30 (2009).

12.	Schueder, F. *et al.* Multiplexed 3D super-resolution imaging of whole cells using spinning disk confocal microscopy and DNA-PAINT. *Nat. Commun.* **8,** (2017).

13.	Auer, A., Strauss, M. T., Schlichthaerle, T. & Jungmann, R. Fast, Background-Free DNA-PAINT Imaging Using FRET-Based Probes. *Nano Lett.* **17,** 6428–6434 (2017).

14.	Lee, J., Park, S., Kang, W. & Hohng, S. Accelerated super-resolution imaging with FRET-PAINT. *Mol. Brain* **10,** 63 (2017).

15.	Chen, F., Tillberg, P. W. & Boyden, E. S. Expansion microscopy. *Science (80-.).* **347,** 543–548 (2015).

16.	Zhao, Y. *et al.* Nanoscale imaging of clinical specimens using pathology-optimized expansion microscopy. *Nat Biotech* **35,** 757–764 (2017).

17. Tillberg, P. W. *et al.* Protein-retention expansion microscopy of cells and tissues labeled using standard fluorescent proteins and antibodies. *Nat. Biotechnol.* **34,** 987–992 (2016).

18. Ku, T. *et al.* Multiplexed and scalable super-resolution imaging of three-dimensional protein localization in size-adjustable tissues. *Nat Biotech* **34,** 973–981 (2016).

19. Chen, F. *et al.* Nanoscale imaging of RNA with expansion microscopy. *Nat. Methods* **13,** 679–684 (2016).

20. Chang, J.-B. *et al.* Iterative expansion microscopy. *Nat. Methods* **14,** (2017).

21. Schermelleh, L., Heintzmann, R. & Leonhardt, H. A guide to super-resolution fluorescence microscopy. *J. Cell Biol.* **190,** 165–175 (2010).

22. Schmidt, R. *et al.* Spherical nanosized focal spot unravels the interior of cells. *Nat. Methods* **5,** 539–544 (2008).

23. Schmidt, R. *et al.* Mitochondrial Cristae Revealed with Focused Light. *Nano Lett.* **9,** 2508–2510 (2009).

24. Juette, M. F. *et al.* Three-dimensional sub–100 nm resolution fluorescence microscopy of thick samples. *Nat. Methods* **5,** 527–529 (2008).

25. Xu, K., Babcock, H. P. & Zhuang, X. Dual-objective STORM reveals three-dimensional filament organization in the actin cytoskeleton. *Nat. Methods* **9,** 185–188 (2012).

26. Urban, N. T., Willig, K. I., Hell, S. W. & Nägerl, U. V. STED Nanoscopy of Actin Dynamics in Synapses Deep Inside Living Brain Slices. *Biophys. J.* **101,** 1277–1284 (2011).

27. Willig, K. I. *et al.* Nanoscopy of Filamentous Actin in Cortical Dendrites of a Living Mouse. *Biophys. J.* **106,** L01–L03 (2014).

28. Westphal, V. *et al.* Video-Rate Far-Field Optical Nanoscopy Dissects Synaptic Vesicle Movement. *Science (80-.).* **320,** 246–249 (2008).

29. Moneron, G. *et al.* Fast STED microscopy with continuous wave fiber lasers. *Opt. Express* **18,** 1302 (2010).

30. Schneider, J. *et al.* Ultrafast, temporally stochastic STED nanoscopy of millisecond dynamics. *Nat. Methods* **12,** 827–830 (2015).

31. Nägerl, U. V., Willig, K. I., Hein, B., Hell, S. W. & Bonhoeffer, T. Live-cell imaging of dendritic spines by STED microscopy. *Proc. Natl. Acad. Sci. U. S. A.* **105,** 18982–7 (2008).

32. Fiolka, R., Shao, L., Rego, E. H., Davidson, M. W. & Gustafsson, M. G. L. Time-lapse two-color 3D imaging of live cells with doubled resolution using structured illumination. *Proc. Natl. Acad. Sci. U. S. A.* **109,** 5311–5 (2012).

33. Shao, L., Kner, P., Rego, E. H. & Gustafsson, M. G. L. Super-resolution 3D microscopy of live whole cells using structured illumination. *Nat. Methods* **8,** 1044–1046 (2011).

34. Jones, S. A., Shim, S.-H., He, J. & Zhuang, X. Fast, three-dimensional super-resolution

imaging of live cells. *Nat. Methods* **8,** 499–505 (2011).

35. Huang, F. *et al.* Video-rate nanoscopy using sCMOS camera–specific single-molecule localization algorithms. *Nat. Methods* **10,** 653–658 (2013).

36. Donnert, G. *et al.* Two-Color Far-Field Fluorescence Nanoscopy. *Biophys. J.* **92,** L67–L69 (2007).

37. Bossi, M. *et al.* Multicolor Far-Field Fluorescence Nanoscopy through Isolated Detection of Distinct Molecular Species. *Nano Lett.* **8,** 2463–2468 (2008).

38. Bückers, J., Wildanger, D., Vicidomini, G., Kastrup, L. & Hell, S. W. Simultaneous multi-lifetime multi-color STED imaging for colocalization analyses. *Opt. Express* **19,** 3130 (2011).

39. Bates, M., Huang, B., Dempsey, G. T. & Zhuang, X. Multicolor super-resolution imaging with photo-switchable fluorescent probes. *Science* **317,** 1749–53 (2007).

40. Shroff, H. *et al.* Dual-color superresolution imaging of genetically expressed probes within individual adhesion complexes. *Proc. Natl. Acad. Sci. U. S. A.* **104,** 20308–13 (2007).

41. Wilmes, S. *et al.* Triple-Color Super-Resolution Imaging of Live Cells: Resolving Submicroscopic Receptor Organization in the Plasma Membrane. *Angew. Chemie Int. Ed.* **51,** 4868–4871 (2012).

42. Hein, B., Willig, K. I. & Hell, S. W. Stimulated emission depletion (STED) nanoscopy of a fluorescent protein-labeled organelle inside a living cell. *Proc. Natl. Acad. Sci. U. S. A.* **105,** 14271–6 (2008).

43. Hess, S. T. *et al.* Dynamic clustered distribution of hemagglutinin resolved at 40 nm in living cell membranes discriminates between raft theories. *Proc. Natl. Acad. Sci. U. S. A.* **104,** 17370–5 (2007).

44. Jungmann, R. *et al.* Multiplexed 3D cellular super-resolution imaging with DNA-PAINT and Exchange-PAINT. *Nat. Methods* **11,** 313–8 (2014).

45. Betzig, E. *et al.* Imaging Intracellular Fluorescent Proteins at Nanometer Resolution. *Science (80-.).* **313,** 1642–1645 (2006).

46. Wang, Y. *et al.* Rapid sequential in situ multiplexing with DNA-Exchange-Imaging in Neuronal Cells and Tissues. *Nano Lett.* acs.nanolett.7b02716 (2017). doi:10.1021/acs.nanolett.7b02716

47. Ertürk, A. *et al.* Three-dimensional imaging of solvent-cleared organs using 3DISCO. *Nat Protoc* **7,** 1983–1995 (2012).

48. Renier, N. *et al.* iDISCO: A Simple, Rapid Method to Immunolabel Large Tissue Samples for Volume Imaging - suppl original. *Cell* **159,** (2014).

49. Ke, M.-T., Fujimoto, S. & Imai, T. SeeDB : a simple and morphology-preserving optical clearing agent for neuronal circuit reconstruction. *Nat. Publ. Gr.* **16,** 1154–1161 (2013).

50.   Aoyagi, Y., Kawakami, R., Osanai, H., Hibi, T. & Nemoto, T. A rapid optical clearing protocol using 2,2'-thiodiethanol for microscopic observation of fixed mouse brain. *PLoS One* **10,** 1–13 (2015).

51.   Costantini, I. *et al.* A versatile clearing agent for multi-modal brain imaging. *Sci. Rep.* **5,** 9808 (2015).

52.   Hama, H. *et al.* Scale: a chemical approach for fluorescence imaging and reconstruction of transparent mouse brain. *Nat. Neurosci.* **14,** 1481–8 (2011).

53.   Hama, H. *et al.* ScaleS: an optical clearing palette for biological imaging. *Nat. Neurosci.* **18,** 1518–1529 (2015).

54.   Susaki, E. A. *et al.* Whole-brain imaging with single-cell resolution using chemical cocktails and computational analysis. *Cell* **157,** 726–739 (2014).

55.   Murakami, T. C. *et al.* A three-dimensional single-cell-resolution whole-brain atlas using CUBIC-X expansion microscopy and tissue clearing. *Nat. Neurosci.* **21,** 625 (2018).

56.   Chung, K. *et al.* Structural and molecular interrogation of intact biological systems. *Nature* **497,** 332–7 (2013).

57.   Tomer, R., Ye, L., Hsueh, B. & Deisseroth, K. Advanced CLARITY for rapid and high-resolution imaging of intact tissues. *Nat. Protoc.* **9,** 1682–97 (2014).

58.   Treweek, J. B. *et al.* Whole-body tissue stabilization and selective extractions via tissue-hydrogel hybrids for high-resolution intact circuit mapping and phenotyping. *Nat. Protoc.* **10,** 1860–1896 (2015).

59.   Yang, B. *et al.* Single-cell phenotyping within transparent intact tissue through whole-body clearing. *Cell* **158,** 945–958 (2014).

60.   Chozinski, T. J. *et al.* Expansion microscopy with conventional antibodies and fluorescent proteins. *Nat. Methods* (2016). doi:10.1038/nmeth.3833

61.   Hell, S. W. & Wichmann, J. Breaking the diffraction resolution limit by stimulated emission: stimulated-emission-depletion fluorescence microscopy. *Opt. Lett.* **19,** 780–2 (1994).

62.   Klar, T. A., Jakobs, S., Dyba, M., Egner, A. & Hell, S. W. Fluorescence microscopy with diffraction resolution barrier broken by stimulated emission. *Proc. Natl. Acad. Sci. U. S. A.* **97,** 8206–10 (2000).

63.   Hofmann, M., Eggeling, C., Jakobs, S. & Hell, S. W. Breaking the diffraction barrier in fluorescence microscopy at low light intensities by using reversibly photoswitchable proteins. *Proc. Natl. Acad. Sci.* **102,** 17565–17569 (2005).

64.   Gustafsson, M. G. Surpassing the lateral resolution limit by a factor of two using structured illumination microscopy. *J. Microsc.* **198,** 82–7 (2000).

65.   Heintzmann, R. & Cremer, C. G. Laterally modulated excitation microscopy: improvement of resolution by using a diffraction grating. in *Proc. SPIE* (eds. Bigio, I. J., Schneckenburger, H., Slavik, J., Svanberg, K. & Viallet, P. M.) **3568,** 185–196

(International Society for Optics and Photonics, 1999).

66. Hess, S. T., Girirajan, T. P. K. & Mason, M. D. Ultra-high resolution imaging by fluorescence photoactivation localization microscopy. *Biophys. J.* **91,** 4258–72 (2006).

67. Rust, M. J., Bates, M. & Zhuang, X. Sub-diffraction-limit imaging by stochastic optical reconstruction microscopy (STORM). *Nat. Methods* **3,** 793–796 (2006).

68. Jungmann, R. *et al.* Single-molecule kinetics and super-resolution microscopy by fluorescence imaging of transient binding on DNA origami. *Nano Lett.* **10,** 4756–61 (2010).

69. ExpansionMicroscopy.org: Physical Specimen Expansion Enabling 3-D Large Volume, Nanoscale Imaging.

70. Gao, R., Asano, S. M. & Boyden, E. S. Q&A Expansion Microscopy. *BMC Biol.* (2017). doi:10.1073/pnas.1617699113

71. Karagiannis, E. & Boyden, E. Expansion microscopy: development and neuroscience applications. *Curr Opin Neurobiol* **50,** 56–63 (2018).

72. Cohen, Y., Ramon, O., Kopelman, I. J. & Mizrahi, S. Characterization of inhomogeneous polyacrylamide hydrogels. *J. Polym. Sci. Part B Polym. Phys.* **30,** 1055–1067 (1992).

73. Raab, M. *et al.* Using DNA origami nanorulers as traceable distance measurement standards and nanoscopic benchmark structures. *Sci. Rep.* **8,** 1780 (2018).

74. Scheible, M. B. & Tinnefeld, P. Quantifying Expansion Microscopy with DNA Origami Expansion Nanorulers. *Biorxiv* (2018). doi:10.1101/265405

75. Bale, J. B. *et al.* Accurate design of megadalton-scale two-component icosahedral protein complexes. *Science* **353,** 389–94 (2016).

76. Richardson, D. S. & Lichtman, J. W. Clarifying Tissue Clearing. *Cell* **162,** 246–257 (2015).

77. Dodt, H.-U. *et al.* Ultramicroscopy: three-dimensional visualization of neuronal networks in the whole mouse brain. *Nat. Methods* **4,** 331–336 (2007).

78. Hausen, P. & Dreyer, C. The Use of Polyacrylamide as an Embedding Medium for Immunohistochemical Studies of Embryonic Tissues. *Stain Technol.* **56,** 287–293 (1981).